Journal of Power Sources 185 (2008) 1022–1029

Contents lists available at ScienceDirect

Journal of Power Sources

journal homepage: www.elsevier.com/locate/jpowsour

Modeling and simulation of a single direct carbon fuel cell

Qinghua Liu[a,b], Ye Tian[a], Chun Xia[a], Levi T. Thompson[b], Bin Liang[c], Yongdan Li[a,*]

[a] Tianjin Key Laboratory of Catalysis Science and Technology and State Key Laboratory for Chemical Engineering (Tianjin University), School of Chemical Engineering, Tianjin University, Weijin Road 92, Tianjin 300072, China
[b] Department of Chemical Engineering, University of Michigan, Ann Arbor 48109-2136, United States
[c] College of Chemical Engineering, Sichuan University, Chengdu 610065, China

ARTICLE INFO

Article history:
Received 15 June 2008
Received in revised form 27 August 2008
Accepted 28 August 2008
Available online 12 September 2008

Keywords:
Direct carbon fuel cell
Carbon
Modeling
Polarization losses
Efficiency

ABSTRACT

A mathematical model was developed to simulate the performance of a direct carbon fuel cell. The model takes account of the electrochemical reaction dynamics, mass-transfer and the electrode processes. An improved packed bed anode was adopted. Polarization losses for the cell components were examined supposing graphite as the fuel and molten carbonate as the electrolyte. The results indicated that the anode activation polarization was the major potential loss in 923–1023 K. The effects of temperature, anode dimension, and carbon particle size on the cell performance were investigated. The model predicted that the power density can be as high as 200–500 W m^{-2}, with carbon particle size in the range 1.0×10^{-7} to 1.0×10^{-4} m and in 923–1023 K and that the overall efficiency of the cell is higher than 55% for low current density and is 45–50% for high current density.

1. Introduction

Factors that impact the development of an energy system include the availability of fuel, efficiency and environmental effect [1]. Fuel cells have a high efficiency for converting chemical energy to electrical energy. These devices are not limited by theoretical Carnot cycle efficiencies [2]. They also typically do not emit pollutants, such as NO_x, SO_x, etc. [3].

Since fuel cells were discovered by William Grove in 1839, a family of fuel cells has been developed [4], which include gaseous hydrogen, methane, methanol, ethanol, and solid carbon [5–10]. Hydrogen fuel cells are technically mature and have been applied in space explorations and are starting to replace the internal combustion engines in automobiles [11]. There has been renewed interest on direct carbon fuel cell (DCFC), which uses solid carbon as the fuel, due to their potential to use coal and coal derivatives as fuel and high thermal efficiency [8–10]. The principle reaction is

$$C + O_2 \rightarrow CO_2 \quad \Delta H^{973} = 395\ \text{kJ mol}^{-1} \tag{1}$$

The theoretical thermal efficiency of DCFC is almost 100% [8,10]. The DCFC is a high temperature device and shares features with a molten carbonate fuel cell (MCFC) and a solid oxide fuel cell (SOFC) [12–21].

The first DCFC prototype was established by Jacques more than 110 years ago [13]. However, the research on this device was intermittent in the early 20th century because of substantial improvements in the efficiencies of steam power plants. In the 1970s, the concept was verified by Weaver and coworkers [14,15]. Since then, there has been substantial progress in the development of high temperature fuel cells including MCFCs and SOFCs. Concepts, materials and processes proved with these fuel cells were applied to DCFC and lead to some major breakthroughs [8,9]. Cherepy et al. [8] investigated the effect of carbon nanostructure on the electrochemical reactivity and found that "turbostratic" carbon, with a high degree of disorder in structure and domain sizes in the range of 30–100 nm, performed the best. They tested a five-cell self-feeding bipolar stack and designed a larger scale system for clean coal. Tao [19] employed a sophisticated configuration which used a liquid tin anode and a YSZ electrolyte. Lipilin et al. [21] established a device combining the features of SOFC and MCFC technology, in which a circulating liquid-molten-salt electrolyte and a carbon-rich fuel were used, and a power density 100 mW cm^{-2} was achieved. Steinberg [20], Hemmes and Houwing [22] carried out macroscopic energy and exergy analyses of a DCFC system. Agarwal and Kornhauser [23] examined an integrated-DCFC-HPBR (hydrogen plasma black reactor) system. However, these modeling studies did not account for the electrode processes in the DCFC. Understanding of the electrode reactions, mass and heat transfers in the device, and the efficiency analyses models for DCFC including the electrode processes are needed.

* Corresponding author. Tel.: +86 22 27405613; fax: +86 22 27405243.
E-mail address: ydli@tju.edu.cn (Y. Li).

0378-7753/$ – see front matter © 2008 Elsevier B.V. All rights reserved.
doi:10.1016/j.jpowsour.2008.08.100

Nomenclature

A	a kinetic parameter related with Ohmic resistance ($\Omega\,m^2\,Pa^{0.67}$)
b	diameter of the contact area between two carbon particles (m)
B	a kinetic parameter related with Ohmic resistance (K)
C	concentration ($mol\,m^{-3}$)
C_{CO_2}	CO_2 concentration in gas phase ($mol\,m^{-3}$)
C_R	a constant related with Ohmic resistance of the contacts ($\Omega\,m^2$)
D	a kinetic parameter related with electrolyte content in the matrix ($\Omega\,m^2$)
D_c	diameter of carbon particle (m)
E_a	apparent activation energy of the electrolyte conductivity ($J\,mol^{-1}$)
f	a kinetic parameter related with Ohmic resistance (K)
F	mechanical force (N)
F'	Faraday's constant (96,487 $C\,mol^{-1}$)
F_f	buoyancy force (N)
F_g	gravitational force (N)
F_r	repulsive force (N)
G	Gibbs-free energy (J)
H	enthalpy (J)
i	order number of a slab
I	current (A)
I_f	measured current (A)
I_t	theoretical current (A)
j	current density ($A\,m^{-2}$)
j_c	current density in the electrode phase ($A\,m^{-2}$)
j_{lim}	limiting current density ($A\,m^{-2}$)
j_s	current density in the electrolyte phase ($A\,m^{-2}$)
j_0	exchange current density ($A\,m^{-2}$)
j_0^0	concentration-independent exchange current density ($A\,m^{-2}$)
K	mass transport coefficient ($m\,s^{-1}$)
n	numbers of electrical charge transfer in an electrochemical reaction (mole)
N_l	number of the carbon particles in each slab
N_s	number of slabs
p_m	mean yield pressure of the asperities (Pa)
P	pressure in gas phase (Pa)
P_{CO_2}	partial pressure of CO_2 in gas phase (Pa)
P_{O_2}	partial pressure of O_2 in gas phase (Pa)
r_1	power of CO_2 partial pressure for the exchange current density equation in cathode
r_2	power of O_2 partial pressure for the exchange current density equation in cathode
R	resistance ($\Omega\,m^2$)
R_c	resistance in the electrode phase ($\Omega\,m^2$)
R_{ce}	resistance of all components except for anode ($\Omega\,m^2$)
R_{cr}	constriction resistance of the electrode phase ($\Omega\,m^2$)
R_{ct}	charge transfer resistance ($\Omega\,m^2$)
R_f	film resistance ($\Omega\,m^2$)
R_s	resistance in the electrolyte ($\Omega\,m^2$)
R'	gas constant ($8.314\,J\,mol\,K^{-1}$)
s	contact area between two carbon particles (m^2)
S	entropy ($J\,K^{-1}$)
T	temperature (K)
V_{cell}	cell voltage (V)
V_N	open circuit voltage (V)
V^0	open circuit voltage at standard state in Eq. (10) (V)
x	height of the packed bed anode (m)
y	length of the packed bed anode (m)
z	width of the packed bed anode (m)

Greek letters

β	apparent charge transfer-coefficient
γ	efficiency
γ_f	current efficiency
γ_t	theoretical reversible efficiency
γ_v	voltage efficiency
ε	voidage of the packed bed
η	polarization loss (V)
η_{act}	activation polarization (V)
η_{con}	concentration polarization (V)
η_{ohm}	Ohmic polarization (V)
σ_c	conductivity of the electrode ($S\,m^{-2}$)
σ_s	conductivity of the electrolyte ($S\,m^{-2}$)
σ_s^0	a pre-exponential factor ($S\,m^{-2}$)

Superscript

b	bulk
0	standard state

Subscript

act	activation
an	anode
cat	cathode
con	concentration
lim	limit
ohm	Ohmic

Work described in this paper focuses on the development of a preliminary mathematical model describing the performance of a DCFC single cell. The purpose is to determine and simulate the various polarizations, V–j relation, power density and efficiencies of the cell. A commercial software MATLAB™ is adopted for this purpose.

2. Model

2.1. System configuration

Previous literature [8] assumed that the collision of carbon particles in the anode transfers the current. However, this mechanism requires an unrealistically high collision frequency to account for the experimental results [24]. In this work, we propose an alternative packed bed model which offers a simplified configuration for the DCFC anode.

Fig. 1 gives an illustration of a DCFC single cell. It consists of three key components, the anode, the cathode, and the electrolyte matrix. Solid carbon fuel is fed into the anode in the form of particles and wetted with molten salt. Each particle is assumed to act as a rigid sphere and packed with a simple hexagonal pattern. The bed consists of several slabs of spherical carbon particles. The number N_s of the slabs is dependent on the bed height x and the diameter of the carbon particle D_c

$$N_s = \frac{x}{D_c} \tag{2}$$

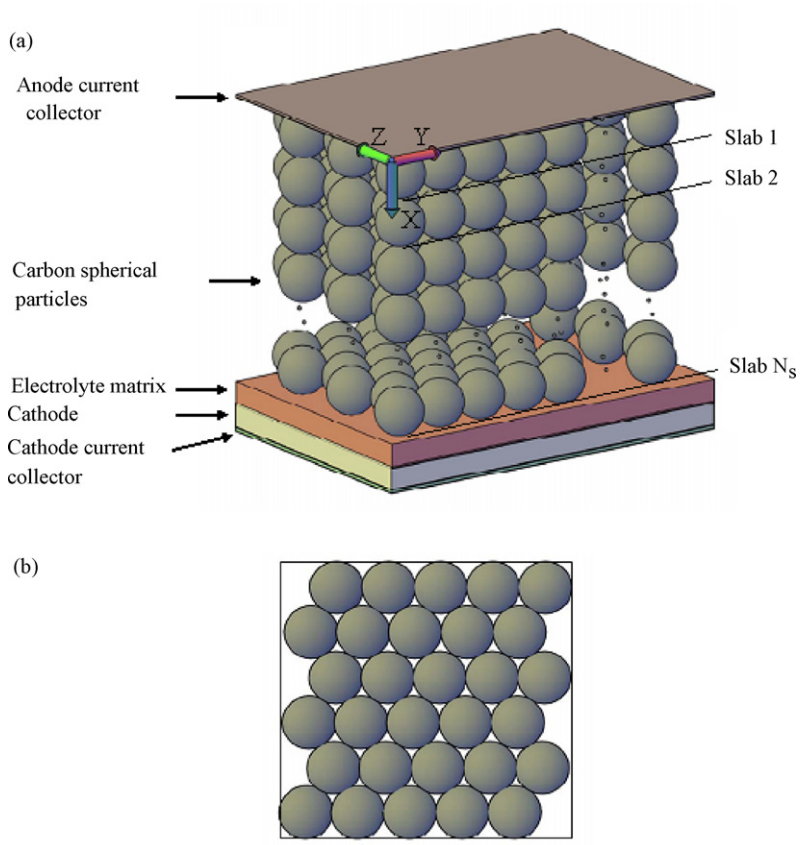

Fig. 1. (a) Schematic configuration of the DCFC single cell using packed bed anode, (b) top view of packed bed electrode.

The number N_l of the particles in each slab is

$$N_l = \frac{1.14yz}{D_c^2} \tag{3}$$

The anode reaction takes place at the interface of carbon and carbonate melt, with release of CO_2 and electrons. The electrolyte matrix is made of a porous ceramic membrane filled with molten carbonate, which allows the migration of carbonate ions from the cathode compartment to the anode compartment. The structure of the cathode is similar to the one adopted in a MCFC. A mixture of air and CO_2 with a ratio of O_2 to CO_2 1:2 is introduced into the cathode.

2.2. Electrode processes

Molten carbonate is a promising electrolyte for the electrochemical oxidation of carbon [8,14,15]. In this work, a Li_2CO_3/K_2CO_3 eutectic melt with a molar ratio of 32:68 is employed as the electrolyte. Graphite is employed as the anode fuel. The anode reactions are as follows:

$$C + 2CO_3^{2-} \rightarrow 3CO_2 + 4e^- \tag{4}$$

$$2C + CO_3^{2-} \rightarrow 3CO + 2e^- \tag{5}$$

The reverse of Boudouard reaction

$$CO_2 + C \rightarrow 2CO \tag{6}$$

is a major side reaction and lowers the efficiency. CO_3^{2-} ions are produced in the lithium doped NiO-based porous cathode where the following reduction reaction occurs

$$2CO_2 + O_2 + 4e^- \rightarrow 2CO_3^{2-} \tag{7}$$

The CO_3^{2-} ions travel across the electrolyte matrix to the anode and the overall cell reactions are

$$C + O_2 \rightarrow CO_2 \tag{8}$$

$$2C + O_2 \rightarrow 2CO \tag{9}$$

The ratio of CO_2/CO produced depends on the thermodynamic and kinetic factors. According to published experimental results, CO_2 is the major gas released from anode in the temperature range 923–1073 K and the CO_2 concentration exceeds that predicted by thermodynamic equilibrium [25–27]. In this work, the production of CO in the anode is not considered. Therefore, reactions (5), (6) and (9) are ignored and the anode reactions are simplified as a four-electron ($n = 4$) process, i.e. reaction (1).

2.3. Electrochemical thermodynamic equations

The open circuit voltage V_N is calculated with Nernst equation that is given by

$$V_N = V^0 + \frac{R'T}{nF'} \ln\left(\frac{p_{O_2} p_{CO_2,cat}^2}{p_{CO_2,an}^3}\right) \tag{10}$$

The open circuit voltage at standard state V^0 can be calculated by

$$V^0 = \frac{\Delta G^0}{nF'} \tag{11}$$

2.4. Polarization losses

When current flows in the cell, the voltage decreases. This phenomenon is well known as the polarization loss η, which is caused

by different mechanisms including charge transfer η_{act}, ion concentration gradient η_{con}, and circuit Ohmic resistance η_{ohm}. Therefore, the cell voltage η_{cell} is determined by subtracting these polarization losses from the open circuit voltage

$$V_{cell} = V_N - (\eta_{act,an} + \eta_{act,cat} + \eta_{ohm} + \eta_{con,an} + \eta_{con,cat}) \quad (12)$$

2.4.1. Activation polarization

In order to simulate the charge transfer processes, the general Bulter–Volmer equation was used to calculate the activation polarizations for anode and cathode, respectively

$$j = j_0 \left\{ \exp\left(\beta \frac{nF'\eta_{act}}{R'T}\right) - \exp\left[-(1-\beta)\frac{nF'\eta_{act}}{R'T}\right]\right\} \quad (13)$$

The apparent charge transfer-coefficient β takes value in the range 0–1, depending on the symmetry of the transition state in the electrochemical reaction, and is typically assigned as 0.5 for fuel cells [28]. The anode exchange current density $j_{0,an}$ is related to the charge transfer resistance R_{ct} and is given by

$$j_{0,an} = \frac{R'T}{nF'R_{ct}} \quad (14)$$

and

$$R_{ct} = 30.79 + 1.48 \ \exp\left(-\frac{T}{28.58}\right) \quad (15)$$

The values in Eq. (15) are obtained from a regression analysis on the data published by Peelen et al. [29].

For the cathode, there is no model that fits all the experimental data. In this work, the model based on the peroxide mechanism is selected [30]

$$j_{0,cat} = j^0_{0,cat}(p_{CO_2})^{r_1}(p_{O_2})^{r_2} \quad (16)$$

The values of $j^0_{0,cat}$, r_1 and r_2 were taken from [31].

2.4.2. Ohmic polarization

Ohmic polarization is caused by resistances inside the cell and obeys Ohm's law. For the anode, the resistance in each slab contains two parts, i.e. the resistances in the electrolyte $R_{s,i}$ and in the electrode $R_{c,i}$ in slab i, respectively [32]. The $R_{s,i}$ is expressed as

$$R_{s,i} = \frac{D_c}{\sigma_s yz\varepsilon^{1.5}} \quad (17)$$

The conductivity of the electrolyte σ_s is a function of temperature and obeys Arrhenius' law. Here the parameters were extrapolated to 923 K [33]

$$\sigma_s = \sigma^0_s \exp\left(-\frac{E_a}{R'T}\right) \quad (18)$$

The current flow through the electrolyte phase is

$$j_{s,i} = j\left[1 - 2\pi\left(\frac{x}{D_c - 1}\right)\right] \quad (19)$$

and the current flow through the electrode phase is

$$j_{c,i} = 2\pi j\left(\frac{x}{D_c - 1}\right) \quad (20)$$

$R_{c,i}$ consists of the constriction resistance, $R_{cr,i}$, and the film resistance, $R_{f,i}$ on the electrode surface. However, for the fresh carbon particle, the contact resistance of two carbon particles is the same as its constriction resistance and is related to the conductivity of the carbon particle σ_c and the diameter of the contact area between two particles b [34]

$$R_{c,i} = R_{cr,i} = \frac{1}{\sigma_c b_i} \quad (21)$$

The contact area s is dependent on the force F acting on the particles and the mean yield pressure of the asperities p_m

$$s_i = \pi b_i^2 \quad (22)$$

$$s_i = \frac{F_i}{p_m} \quad (23)$$

The forces applied on the particles include gravitational force $F_{g,i}$, buoyancy force $F_{f,i}$ and repulsive force $F_{r,i}$. However, the repulsive force on the top and the bottom of carbon particle is assumed to be equal. Consequently, the difference of gravitational force and buoyancy force is the force pressing the particles

$$F_i = (N_s - 1)(F_{f,i} - F_{g,i}) \quad (24)$$

$$F_{f,i} = 1.33\rho_s \pi g (D_c)^2 \quad (25)$$

$$F_{g,i} = 1.33\rho_c \pi g (D_c)^2 \quad (26)$$

The resistances of the other parts can be expressed as follows [35]:

$$R_{ce} = \frac{A}{p^{0.67}_{O_2}} \exp\left(\frac{B}{T}\right) + C_R + D \ \exp\left(\frac{f}{T}\right) \quad (27)$$

where p_{O_2} is the partial pressure of oxygen at cathode surface, C_R is a constant related with Ohmic resistance of the contacts, D is a kinetic parameter which is proportional to the electrolyte content of the matrix. The overall Ohmic polarization can be express as

$$\eta_{ohm} = jR_{ce} + \eta_{ohm,an} \quad (28)$$

$$\eta_{ohm,an} = \sum_{i=1}^{N_s} j_{s,i}R_{s,i} + \sum_{i=1}^{N_s} j_{c,i}R_{c,i} \quad (29)$$

2.4.3. Concentration polarization

The reactant transport resistances lead to a concentration polarization. The concentration polarization can be measured using a limiting current density method as described below [36]

$$\eta_{con,cat} = \frac{R'T}{nF'} \ln\left(1 - \frac{j}{j_{lim}}\right) \quad (30)$$

In a DCFC, the phenomenon of current saturation does not occur, because solid carbon is always in excess at the anode [26,29]. As a consequence, the concentration polarization of the anode is negligible. The cathode is porous, and the partial pressures of gases at the interface are lower than in the bulk gas phase when the current density is high. The cathode concentration polarization can be calculated as

$$j_{lim,cat} = nF'K_{CO_2}C^b_{CO_2} \quad (31)$$

The mass transport coefficient K_{CO_2} is taken as 3.5×10^{-2} m s^{-1} [37].

2.5. Efficiencies

The operating efficiency is lowered by activation, Ohmic, and mass transport polarizations. The theoretical reversible efficiency of a fuel cell can be expressed as the function of the total free energy and enthalpy changes:

$$\gamma_t = \frac{\Delta G}{\Delta H} \quad (32)$$

The overall efficiency is defined as:

$$\gamma = \gamma_t\gamma_v\gamma_f \quad (33)$$

Table 1
Setting parameters used in simulation

Parameter	Value	Reference
Total gas pressure in anode (Pa)	1.01325×10^5	
Total gas pressure in cathode (Pa)	1.01325×10^5	
Height of packed bed anode, x (m)	1.0×10^{-7} to 1.0×10^{-3}	
Length of packed bed anode, y (m)	1.0×10^{-2}	
Width of packed bed anode, z (m)	1.0×10^{-2}	
Diameter of spherical graphite particle, D_c (m)	1.0×10^{-7} to 1.0×10^{-4}	
Voidage of packed bed anode, ε	0.396	
Cathode material	$Li_xNi_{1-x}O$	[30]
Cathode thickness (m)	0.5×10^{-3}	[30]
Electrolyte composition (mol%)	$62Li_2CO_3/38K_2CO_3$	
Matrix thickness (m)	0.5×10^{-3}	[30]
Matrix material	γ-$LiAlO_2$	[30]
Cell operating temperature T (K)	923–1023	
Fuel	Graphite	
Conductivity of graphite particle, σ_c ($S\,m^{-2}$)	1.6×10^5	[36]
Density of graphite particle, ρ_c ($kg\,m^{-3}$)	1.5×10^3	[36]
Density of electrolyte, ρ_s ($kg\,m^{-3}$)	2.0×10^3	[33]
Mass transport coefficient of CO_2, K_{CO_2} ($m\,s^{-1}$)	3.5×10^{-2}	[32]
Apparent activation energy E_a for Eq. (18) ($J\,mol^{-1}$)	2.191×10^4	[33]
Pre-exponential factor σ_s^0 for Eq. (18) ($S\,m^{-2}$)	2.322×10^5	[33]
Apparent charge transfer-coefficient, β	0.5	
Concentration-independent exchange current density, $j_{0,cat}^0$ ($A\,m^{-2}$)	5.0×10^2	[35]
Power of CO_2 partial pressure for the exchange current density equation in cathode, r_1	−1.250	[34]
Power of O_2 partial pressure for the exchange current density equation in cathode, r_2	0.375	[34]

where γ_v is the voltage efficiency given by:

$$\gamma_v = \frac{V_{cell}}{V_N} \tag{34}$$

and γ_f is the current efficiency written as:

$$\gamma_f = \frac{I_f}{I_t} \tag{35}$$

2.6. Further assumptions

All parameters used in this work are summarized in Table 1. Three additional assumptions for the simulation include:

- Air consists of 75.67% N_2, 20.35% O_2, 3.03% H_2O, 0.92% Ar, and 0.03% CO_2 and all the components are regarded as ideal gas.
- The operation temperature of the DCFC is in the range 923–1023 K.
- The whole surface of the spherical graphite particle is effective in the anode.

3. Results and discussion

3.1. Thermodynamic properties

The open circuit voltage V_N is a primary parameter for the performance of a fuel cell. Generally, DCFC operates at the atmospheric pressure and air is used in the cathode. Consequently, the open circuit voltage V_N depends only on the working temperature. As shown in Fig. 2, V_N decreases slightly with the increase of the temperature and is beyond 0.87 V in 873–1173 K.

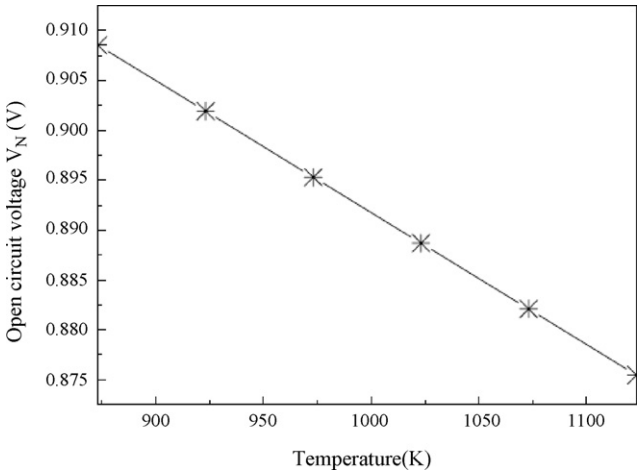

Fig. 2. Open circuit voltage vs. temperature.

3.2. Electrochemical dynamic characteristics

Figs. 3–6 illustrate the contributions of various polarizations as a function of temperature for a single cell in 923–1023 K and based on $x = 1.0 \times 10^{-3}$ m, $y = z = 1.0 \times 10^{-2}$ m, $D_c = 1.0 \times 10^{-5}$ m. These results indicate that the cathode activation polarization loss is close to the cathode concentration polarization, and both are much lower than the anode activation polarization loss. The anode Ohmic polarization is in the same order of magnitude as the anode activation polarization.

3.3. Effect of temperature

The open circuit voltage decreases about 0.015 V along with the temperature increases from 923 to 1023 K. All the polarization losses examined show strong dependence on the temperature. The increase of temperature lowers the anode activation loss effectively, but increases the cathode activation loss slightly. The concentration loss increases a little with the increase of the temperature, while the Ohmic polarization loss shows a slight dependence on the temperature.

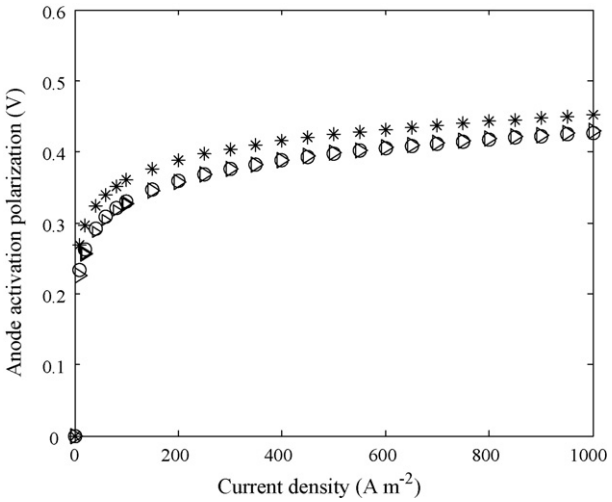

Fig. 3. Anode activation polarization loss vs. current density in 923–1023 K. (✳) at 923 K, (○) at 973 K, (>) at 1023 K.

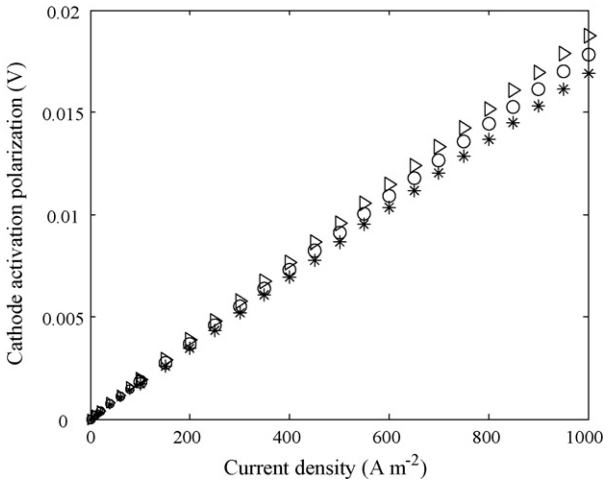

Fig. 4. Cathode activation polarization loss vs. current density in 923–1023 K. (✳) at 923 K, (○) at 973 K, (>) at 1023 K.

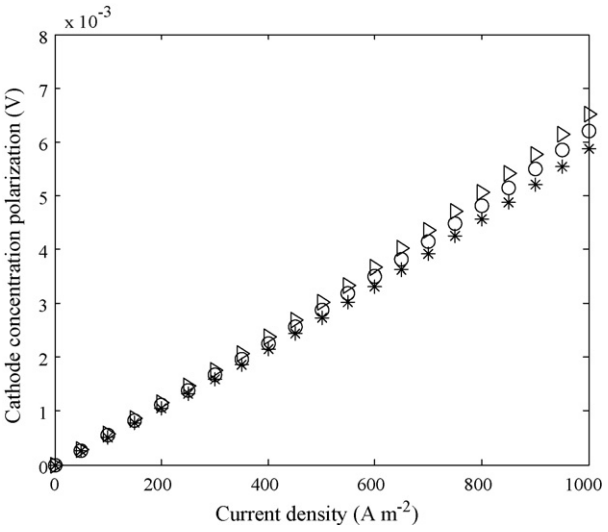

Fig. 5. Cathode concentration polarization loss vs. current density in 923–1023 K. (✳) at 923 K, (○) at 973 K, (>) at 1023 K.

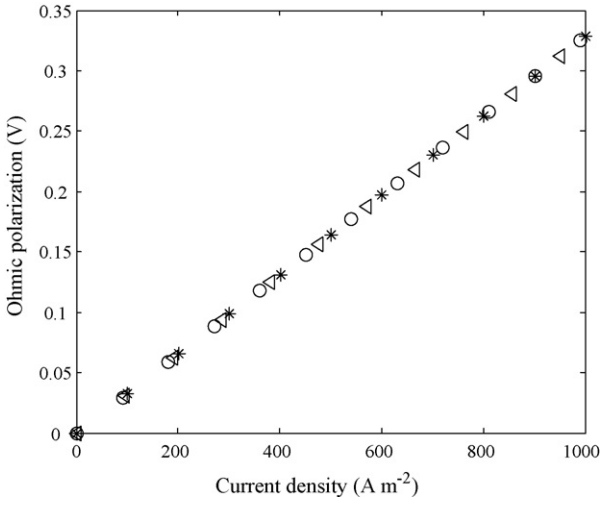

Fig. 6. Ohmic polarization loss vs. current density in 923–1023 K. (✳) at 923 K, (○) at 973 K, (>) at 1023 K.

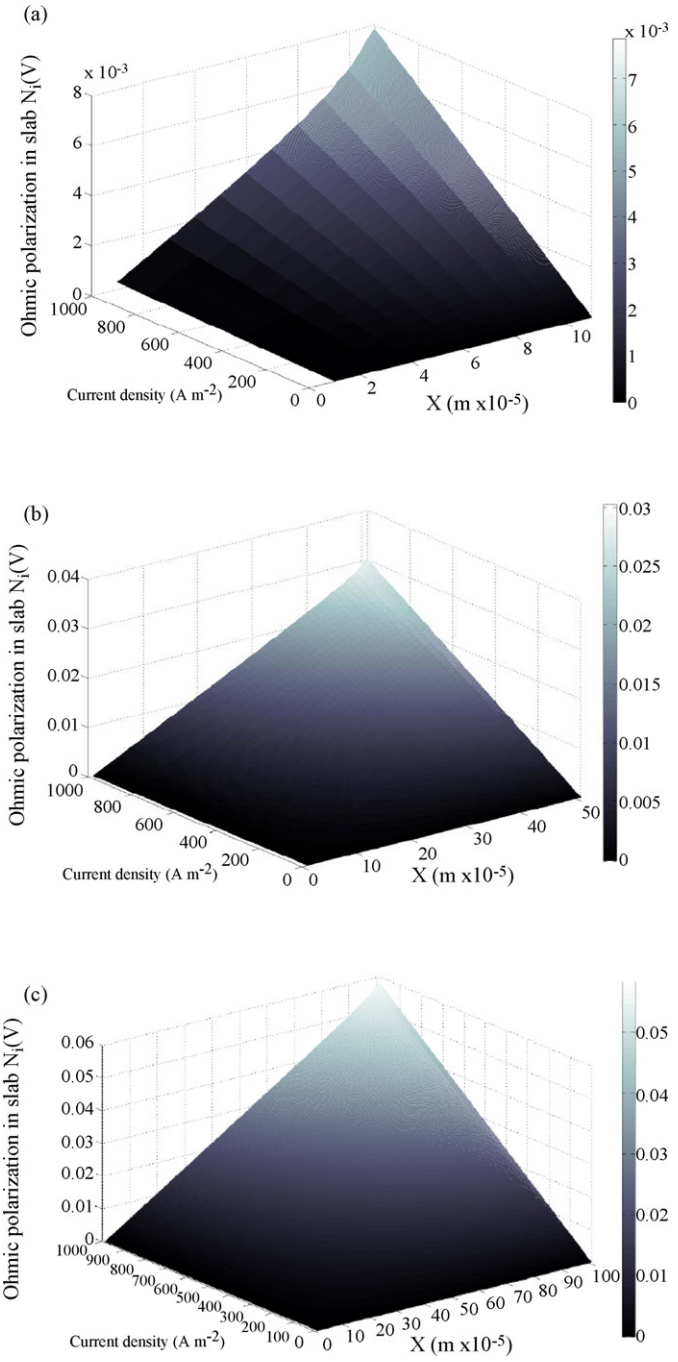

Fig. 7. Effect of height of packed bed anode on Ohmic polarization in slab N_i at 973 K with $D_c = 1 \times 10^{-5}$ m. (a) $N_s = 10$; (b) $N_s = 50$; (c) $N_s = 100$.

3.4. Effect of anode dimension and particle size

The voltage drop in the anode electrode contributes the major part of the Ohmic polarization losses from all the components, which depends on the anode dimension and the carbon particle size. Here we examine three parameters of the anode dimensions: the height x, the length y and the width z of the packed bed anode. Because each carbon particle acts like an electrode, the voltage drop in the anode is independent of y and z. As a consequence, the x decides the anode voltage drop. In Fig. 7, the Ohmic polarization loss in each slab is plotted as the function of current density and bed height x. The sum of voltage drop in each slab is the total anode

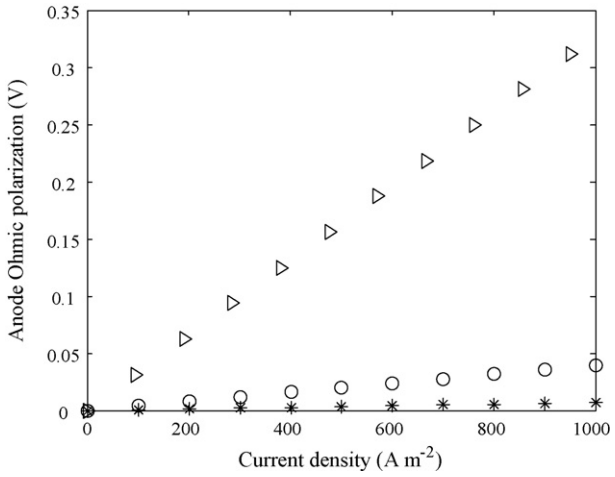

Fig. 8. Effect of carbon particle size on anode Ohmic polarization at 973 K. (✳) $D_c = 1 \times 10^{-6}$ m, (◯) $D_c = 1 \times 10^{-5}$ m, (>) $D_c = 1 \times 10^{-4}$ m.

Ohmic polarization in the anode. As the bed height increasing, the voltage drop in each slab increases.

The effect of carbon particle size on the anode Ohmic polarization is shown in Fig. 8. In this work, the range of carbon particle size is 1.0×10^{-7} to 1.0×10^{-4} m. The anode Ohmic polarization is <0.05 V when the diameter of carbon particle is $<1.0 \times 10^{-5}$ m and has the same order of magnitude as the Ohmic polarization caused by other components. In the range of 1.0×10^{-5} to 1.0×10^{-4} m, the anode ohmic polarization displays a sharp increase as the increase of the particle size and contributes the major part of Ohmic polarization. If the diameter of carbon particle is $>1.0 \times 10^{-4}$ m, the anode polarization will become much more serious and it is not in the scope of this model.

3.5. V–j relations and power density

Fig. 9 plots the *V–j* relations and powder densities of the single cell at different temperatures. For the two cases with $D_c < 1.0 \times 10^{-4}$ m and the current density <200 A m^{-2}, the voltage is higher than 0.5 V in 923–1023 K. If the current density is >200 A m^{-2}, the voltage is 0.4–0.5 V for the cell using carbon particles with $D_c < 1.0 \times 10^{-5}$ m. However, for $D_c > 1.0 \times 10^{-5}$ m, the voltage is lower than 0.4 V. For $D_c \leq 1.0 \times 10^{-5}$ m, the power density in 923–1023 K increases monotonically with the increase of the current density, while for $D_c = 1.0 \times 10^{-4}$ m, the power density shows peaks at 150.2, 178.0 and 202.0 W m^{-2} for 923, 973 and 1023 K, respectively. Also is shown in Fig. 9, the cell voltage and the power density show some dependency on the working temperature.

The results presented here indicate that the performance of a DCFC single cell is under the control of the activation polarization and the Ohmic polarization. The anode activation polarization accounts for the most serious loss, which can be attributed to the low reaction rate of the electrochemical oxidation of graphite. The exchange current density of anode in DCFC is below 10 A m^{-2}, which is rather low if compared to that of the anode in a MCFC in the order of several hundred A m^{-2}. Utilization of carbon with good activity for electrochemical oxidation reaction is a feasible way to overcome this problem [8].

3.6. Efficiencies

The theoretical reversible efficiency of reaction (1) is 100% based on lower heating value for 923, 973 and 1023 K. While for high temperature hydrogen fuel cell, it is only 83% because of the

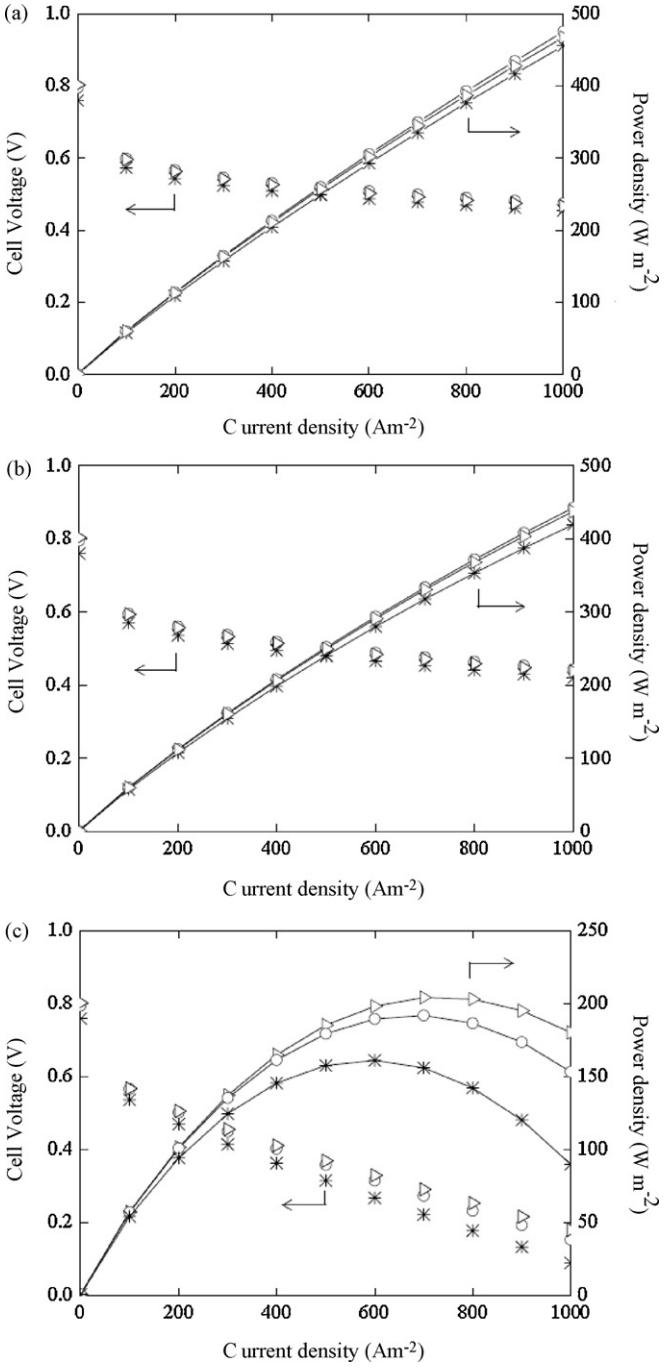

Fig. 9. Cell voltage and power density vs. current density with $N_s = 10$. (a) $D_c = 1 \times 10^{-6}$ m; (b) $D_c = 1 \times 10^{-5}$ m; (c) $D_c = 1 \times 10^{-4}$ m. (✳) $T = 923$, (◯) $T = 973$ K, (>) $T = 1023$ K.

entropy change in the cell reaction under normal operating condition [22]. This is a unique thermodynamic predominance for DCFC.

Different from gaseous or liquid fuels, the concentration of carbon is invariant throughout the reaction process at the anode, and the phenomenon of fuel crossover is inexistent for DCFC. Therefore, γ_f is equal to 100%. However, the voltage efficiency γ_v, is affected by the operating temperature, anode dimension, particle size, and carbon species, etc. Based on the model formulated in this work, an approximate efficiency of DCFC can be given. When the current density is <200 A m^{-2}, the overall efficiency γ is higher than 55%,

and is about 45–50% when the current density is >400 A m^{-2} in 923–1023 K. Finally, it should be noted that this result is based on the DCFC single cell using graphite as fuel, molten Li/K carbonates as the electrolyte and a porous Ni cathode as the one used in a MCFC [8].

4. Conclusions

The performance of a DCFC was simulated. The simulation results reveal several important feathers of the very promising DCFC.

The cell is under the control of anode activation polarization at 923–1023 K due to the low activity of graphite used in this work. The working temperature has a decisive effect on the various polarization losses, especially for the anode activation polarization, which indicates that the anode surface reaction rate is a key factor. The performance of the cell depends strongly on the height of the packed bed anode, and the carbon particle size. This means that the reaction surface area and the transportation path are among the most important factors.

The power density can be as high as 200–500 W m^{-2} with carbon particle size in the range of 1.0×10^{-7} to 1.0×10^{-4} m and in 923–1023 K. The approximate total efficiency of the single cell is higher than 55% for low current density and 45–50% for high current density.

Acknowledgements

This work has been supported by the Natural Science Foundation of China under contract numbers 20425619 and 20736007. The work has been also supported by the Program of Introducing Talents to the University Disciplines under file number B06006, and the Program for Changjiang Scholars and Innovative Research Teams in Universities under file number IRT 0641.

References

[1] J. Briywer, F. Jabbari, E.M. Leal, T. Orr, J. Power Sources 158 (2006) 213–224.
[2] M. Winter, R.J. Brodd, Chem. Rev. 104 (2004) 4245–4269.
[3] K.V. Kordesch, G.R. Simader, Chem. Rev. 95 (1995) 191–207.
[4] S. Srinivasan, Fuel Cells: from Fundamentals to Applications, Springer, NY, USA, 2006, pp. 196–199.
[5] X.M. Ren, M.S. Wilson, S. Golgttesfeld, J. Electrochem. Soc. 143 (1996) L12–L15.
[6] S. Wasmus, A. Küver, J. Electroanal. Chem. 461 (1999) 14–31.
[7] K. Pointon, B. Lakeman, J. Irvine, J. Bradley, S. Jain, J. Power Sources 162 (2006) 750–756.
[8] N.J. Cherepy, R. Krueger, K.J. Fiet, A.F. Jankowski, J.F. Cooper, J. Electrochem. Soc. 152 (2005) A80–A87.
[9] S. Zecevic, E.M. Patton, P. Parhami, Carbon 42 (2004) 1983–1993.
[10] D. Cao, Y. Sun, G. Wang, J. Power Sources 167 (2007) 250–257.
[11] N. Demirdöven, J. Deutch, Science 305 (2004) 974–976.
[12] J.R. Selman, J. Power Sources 160 (2006) 852–857.
[13] W.W. Jacques, US Patent No. 555,551 (1896).
[14] R.D. Weaver, L. Tietz, D. Cubicciotti, Direct use of carbon in a fuel cell: feasibility investigation, Report for USA EPA, Office of R&D, EPA-650/2-75-040, 1975.
[15] R.D. Weaver, S.C. Leach, A.E. Bayce, L. Nanis, Direct electrochemical generation of electricity from Coal, SRI, Menlo Park, CA, USA, Report for SAN-0115/105-1, 1979.
[16] T. Nunoura, K. Dowaki, C. Fushimi, S. Allen, E. Mészáros, M.J. Antal, Ind. Eng. Chem. Res. 46 (2007) 734–744.
[17] T.M. Gür, R.A. Huggins, J. Electrochem. Soc. 139 (1992) L95–L97.
[18] G.A. Hackett, J.W. Zondlo, R. Svensson, J. Power Sources 168 (2007) 111–118.
[19] T.T. Tao, US Patent No. 6,692,861 (2004).
[20] M. Steinberg, Int. J. Hydrogen Energy 31 (2006) 405–411.
[21] A.S. Lipilin, I.I. Balachov, L.H. Dubois, A. Sanjurjo, M.C. McKubre, S. Crouch-Baker, M.D. Hornbostel, F.L. Tanzclla, US Patent Appl. No. 20060019132 (2006).
[22] K. Hemmes, M. Houwing, Proceedings of the 3rd International Conference on Fuel Cell Science Engineering and Technology, Ypsilanti, MI, USA May 23–25, 2005, pp. 499–505.
[23] R. Agarwal, A.A. Kornhauser, Proceedings of the 2004 ASME Heat Transfer/Fluids Engineering Summer Conference, Charlotte, NC, USA July 11–15, 2004, pp. 1–4.
[24] R.E. Plimley, A.R. Wright, Chem. Eng. Sci. 39 (1984) 395–405.
[25] D.G. Vutetakis, Electrochemical oxidation of carbonaceous materials dispersed in molten salt, Ph.D. Dissertation, Ohio State University, Columbus, OH, USA, 1985.
[26] D.G. Vutetakis, D.R. Skidmore, H.J. Byker, J. Electrochem. Soc. 134 (1987) 3027–3035.
[27] V.E. Hauser, A study of carbon anode polarization in fused carbonate fuel cells, Ph.D. Dissertation, Oregon State University, Corvallis, OR, USA, 1964.
[28] S.H. Chan, C.F. Low, O.L. Ding, J. Power Sources 103 (2002) 188–200.
[29] W.H.A. Peelen, M. Olivry, S.F. Au, J.D. Fehribach, K. Hemmes, J. Appl. Electrochem. 30 (2000) 1389–1395.
[30] N. Subramanian, B.S. Haran, P. Ganesan, R.E. White, B.N. Popov, J. Electrochem. Soc. 150 (2003) A46–A56.
[31] J.A. Prins-Jansen, K. Hemmes, J.H.W. De Wit, Electrochim. Acta 42 (1997) 3585–3600.
[32] J.O'M. Bockris, J. Kim, J. Appl. Electrochem. 27 (1997) 890–901.
[33] T. Kojima, Y. Miyazaki, K. Nomura, K. Tanimoto, J. Electrochem. Soc. 154 (2007) F222–F230.
[34] P.G. Slade, Electrical Contacts: Principles and Applications, Marcel Dekker, NY, USA, 1999, pp. 15–44.
[35] B. Bosio, P. Costamagna, F. Parodi, Chem. Eng. Sci. 54 (1999) 2907–2916.
[36] L.I. Antroropov, Theoretical Electrochemistry, Mir Publishers, Moscow, 1977, pp. 331–335.
[37] E. Arato, B. Bosio, P. Costa, F. Parodi, J. Power Sources 102 (2001) 74–81.